LINEAR AND NONLINEAR MODELING OF CYLINDRICAL HYDRODYNAMIC BEARINGS

Jefferson Silva Barbosa

Vinícius Nunes Carvalho

André Beires

Aldemir Ap Cavalini Jr

Valder Steffen Jr

Jheris.barbosa@gmail.com

LMEst - Laboratory of Mechanics and Structures, Federal University of Uberlândia, School of Mechanical Engineering, Av. João Naves de Ávila, 2121, Uberlândia, MG, 38408-196, Brazil.

Abstract: *This paper is dedicated to the analysis of the linear and nonlinear approaches frequently used to model cylindrical hydrodynamic bearings. Regarding the considered nonlinear model, hydrodynamic supporting forces are determined from the solution of the dimensionless Reynolds' equation for cylindrical and short journal bearings. In this case, the nonlinear hydrodynamic forces are applied directly on the rotating shaft. The supporting forces can also be obtained from the linear model, in which stiffness and damping coefficients are determined by imposing small perturbations around the equilibrium position of the rotating shaft (linearization process). The linear hydrodynamic forces are derived from the coefficients related with each bearing. A representative finite element model is used to obtain the dynamic responses of a rotating machine composed by a horizontal flexible shaft, three discs, and two cylindrical hydrodynamic bearings. Additionally, the displacement responses obtained from the nonlinear short bearing theories are compared with the linear long bearing theory.*

Keywords*: rotor dynamics, hydrodynamic journal bearing, linear and nonlinear modeling.*

1 INTRODUCTION

The computational simulation of the dynamic behavior of rotating machines is an important design tool for engineers. It allows a comprehensive understanding about the dynamics of the system, considering the influence of the variables involved in the problem (Meggiolaro, 1996). Thereby, a mathematical model capable of representing satisfactorily the dynamic behavior of a rotating machine is obtained by taking into account various subsystems, as follows: first, the subsystems that are defined by their geometry, such as the shaft, drives and couplings; later, the gyroscopic effect; finally, the subsystems that are frequency and/or state dependent, such as the hydrodynamic bearings. The bearings are one of the most critical subsystems of the rotor system, influencing significantly the performance, life, and reliability of the machine. According to Vance et al. (2010), many problems in rotating systems can be attributed to the design and application of the bearings. Thus, understanding the physical phenomena that involve the bearings is essential to improve the dynamic performance of the system.

The hydrodynamic bearings represent an important component of rotating machinery due to their large use in the industry (Riul, 1988). In this case, the load is supported by a thin film of lubricant that separates the shaft from the bearing (i.e., there is no direct contact between metal parts). Thus, this subsystem can theoretically offer infinite life, considering that the rotor operates under safe dynamic conditions and with clean lubricant (Vance et al., 2010). It is worth mentioning that due to the oil film, the damping effect on hydrodynamic bearings is more pronounced than in rolling bearings, which is beneficial in machines that go through critical speeds during startup and stop down procedures. In this context, the analysis of the linear and nonlinear approaches, frequently used to model cylindrical hydrodynamic bearings, becomes interesting for design purposes, maintenance, and application of structural health monitoring techniques, etc.

2 ROTOR MODELING

Equation (1) presents the differential equation that represents the dynamic behavior of a flexible rotor supported by fluid film bearings (Lalanne and Ferraris, 1998).

$$M\ddot{q} + [D + \Omega D_g]\dot{q} + [K + \dot{\Omega} K_{st}]q = W + F_u + F_s \tag{1}$$

where M is the mass matrix, D is the damping matrix (i.e, proportional damping), D_g represents the gyroscope effect, K is the stiffness matrix, and K_{st} is the stiffness matrix resulting from the transient motion. All these matrices are related to the rotating parts of the system, such as couplings, discs, and the shaft. The vector q is the generalized displacements, and Ω is the shaft rotation speed. W stands for the weight of the rotating parts, F_u represents the unbalance forces, and F_s is the vector of the shaft supporting forces produced by the hydrodynamic bearings. The shaft is modeled by using Timoshenko's beam elements (finite element model) with two nodes and four degrees of freedom per node (i.e., two displacements and two rotations).

3 LINEAR MODELING OF CYLINDRICAL BEARINGS

In this work, the hydrodynamic supporting forces are determined by following the approach proposed by Riul (1988). This linear model is based on the solution of the dimensionless Reynolds' equation for cylindrical journal bearings (Fig. 1), as expressed by Eq. (2). Its solution is obtained by using the finite difference method.

$$\left(\frac{L_h}{R}\right)^2 \frac{\partial^2 \bar{p}_h}{\partial \theta^2} + \frac{3}{\bar{h}_h}\left(\frac{L_h}{R}\right)^2 \left(\frac{\partial \bar{h}_h}{\partial \theta}\right)\frac{\partial \bar{p}_h}{\partial \theta} + \frac{\partial^2 \bar{p}_h}{\partial \bar{y}^2} = \frac{12\pi}{\bar{h}_h^{\,3}}\left[\left(\bar{x} - 2\dot{\bar{z}}\right)\sin\theta - \left(\bar{z} + 2\dot{\bar{x}}\right)\cos\theta\right] \tag{2}$$

where $\bar{p}_h = \bar{p}_h(\theta, \bar{y})$ is the pressure distribution on the bearing (Eq. (3); μ_h is the oil viscosity), $\bar{y}$ is the longitudinal coordinate of the shaft center O_E (on the bearing position), θ is the cylindrical coordinate, R is the shaft radius, L_h is the length of the bearing, and $\bar{h}_h$ is the

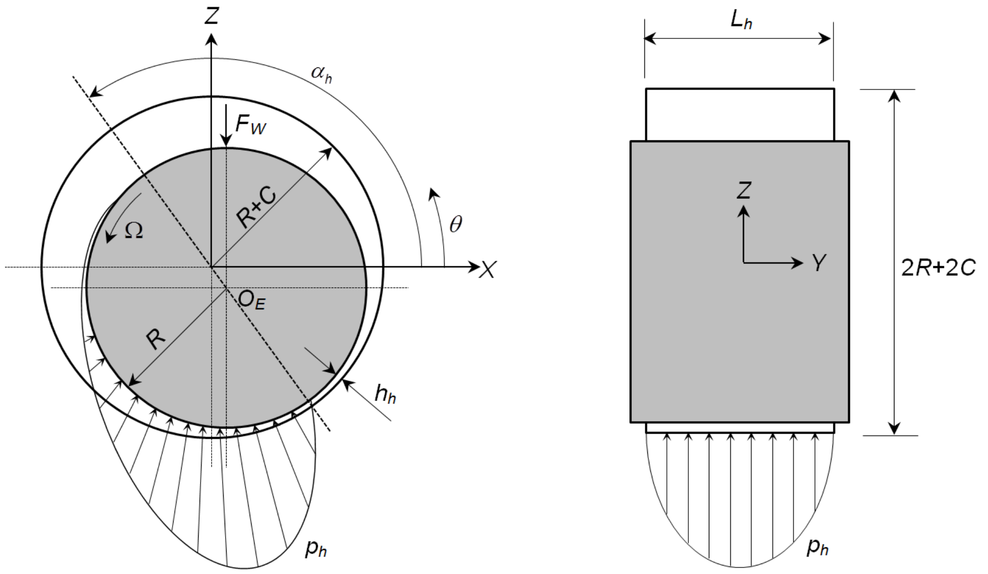

a) XZ-plane **b) YZ-plane**

Figure 1. Cylindrical hydrodynamic bearing

oil film thickness ($\bar{h}_h = 1 - \bar{x}\cos\theta - \bar{z}\sin\theta$); $\bar{x} = x/C$ and $\bar{z} = z/C$ are the coordinates of O_E along the X and Z directions, respectively; $\dot{\bar{x}} = \dot{x}/(\Omega C)$ and $\dot{\bar{z}} = \dot{z}/(\Omega C)$, where C is the radial clearance of the bearing. [$\bar{\cdot}$] is a dimensionless value. The bearing surface is assumed stationary.

$$\bar{p}_h = \frac{p_h}{\mu_h \Omega}\left(\frac{C}{L_h}\right)^2 \tag{3}$$

The hydrodynamic forces $\mathbf{F}_h$ are determined by the integration of Eq. (2) over the bearing supporting area, as given by Eq. (4).

$$F_h = \frac{\mu \Omega R L_h{}^3}{2\pi C^2}\sqrt{F_1{}^2(\bar{x}, z, \dot{\bar{x}}, \dot{\bar{z}}) + F_2{}^2(x, z, \dot{\bar{x}}, \dot{\bar{z}})} \tag{4}$$

where

$$F_1(\bar{x}, z, \dot{\bar{x}}, \dot{\bar{z}}) = -\int_0^1\int_0^{2\pi} \bar{p}_h(\theta, \bar{y})\cos\theta d\theta d\bar{y} \tag{5}$$

$$F_2(x, z, \dot{\bar{x}}, \dot{\bar{z}}) = -\int_0^1\int_0^{2\pi} \bar{p}_h(\theta, \bar{y})\sin\theta d\theta d\bar{y} \tag{6}$$

In order to determine the linearized stiffness coefficients (Riul, 1988), the center of the shaft O_E has been separately displaced from its equilibrium position along the X and Z directions (i.e., small displacements $\Delta\bar{x}$ and $\Delta\bar{z}$, respectively). Consequently, the direct (K_{xx} and K_{zz}) and cross-coupled (K_{xz} and K_{zx}) stiffness coefficients can be obtained for a give operating condition of the bearing. Equation (7) presents the formulation associated with the considered coefficients.

$$
\begin{aligned}
K_{xx} &= -S_S \left(\frac{F_1(\Delta\bar{x}) - F_1(-\Delta\bar{x})}{\Delta\bar{x}} \right) \\
K_{xz} &= -S_S \left(\frac{F_1(\Delta\bar{z}) - F_1(-\Delta\bar{z})}{\Delta\bar{z}} \right) \\
K_{zx} &= -S_S \left(\frac{F_2(\Delta\bar{x}) - F_2(-\Delta\bar{x})}{\Delta\bar{x}} \right) \\
K_{zz} &= -S_S \left(\frac{F_2(\Delta\bar{z}) - F_2(-\Delta\bar{z})}{\Delta\bar{z}} \right)
\end{aligned}
\tag{7}
$$

where *Ss* is the so-called Sommerfield number, as shown the Eq. (8).

$$
S_S = \frac{1}{2\sqrt{F_1^{\,2}(\bar{x}, \bar{z}, \dot{\bar{x}}, \dot{\bar{z}}) + F_2^{\,2}(\bar{x}, \bar{y}, \dot{\bar{x}}, \dot{\bar{z}})}}
\tag{8}
$$

The damping coefficients are determined following in a similar manner, wherein small velocities $\Delta\dot{\bar{x}}$ and $\Delta\dot{\bar{z}}$ are applied along the *X* and *Z* directions, respectively, from the equilibrium position of the shaft. The damping coefficients are presented in Eq. (9).

$$
\begin{aligned}
C_{xx} &= -S_S \left(\frac{F_1(\Delta\dot{\bar{x}}) F_1(-\Delta\dot{\bar{x}})}{\Delta\dot{\bar{x}}} \right) \\
C_{xz} &= -S_S \left(\frac{F_1(\Delta\dot{\bar{z}}) - F_1(-\Delta\dot{\bar{z}})}{\Delta\dot{\bar{z}}} \right) \\
C_{zx} &= -S_S \left(\frac{F_2(\Delta\dot{\bar{x}}) - F_2(-\Delta\dot{\bar{x}})}{\Delta\dot{\bar{x}}} \right) \\
C_{zz} &= -S_S \left(\frac{F_2(\Delta\dot{\bar{z}}) - F_2(-\Delta\dot{\bar{z}})}{\Delta\dot{\bar{z}}} \right)
\end{aligned}
\tag{9}
$$

4 NONLINEAR MODELING OF CYLINDRICAL BEARINGS

In the nonlinear modeling, the hydrodynamic supporting forces are determined by following the approach proposed by Capone (1986). This nonlinear model is based on the solution of the dimensionless Reynolds' equation for cylindrical and short journal bearings (Fig. 1), as expressed by Eq. (10).

$$
\left(\frac{R}{L_h} \right)^2 \frac{\partial}{\partial \bar{y}} \left(\bar{h}_h^3 \frac{\partial \bar{p}_h}{\partial \bar{y}} \right) = \frac{\partial \bar{h}_h}{\partial \theta} + 2\dot{\bar{h}}_h
\tag{10}
$$

where the dimensionless oil film pressure is

$$
\bar{p}_h = \frac{p_h}{6\mu_h \Omega (R / L_h)^2}
\tag{11}
$$

The simplifications applied to Reynolds' equation allow its direct integration, leading to the analytical form of the pressure field (Eq. (12)); $\bar{p}_h(\theta, \pm 0.5) = 0$ are defined as the boundary conditions.

$$\bar{p}_h(\theta,\bar{y}) = \frac{1}{8}\left(\frac{L_h}{R}\right)^2 \left[\frac{(\bar{x} - 2\dot{\bar{z}})\sin\theta - (\bar{z} + 2\dot{\bar{x}})\cos\theta}{\bar{h}_h^{\ 3}}\right](4\bar{y}^2 - 1) \tag{12}$$

The hydrodynamic forces F$_h$ are determined by the integration of Eq. (12) over the bearing supporting area.

$$F_h = -\frac{6\mu\Omega R^3}{8}\int_{-1/2}^{1/2}\int_{\alpha_h}^{\alpha_h+\pi} \bar{p}_h(\theta,\bar{y})\begin{bmatrix}\cos\theta \\ \sin\theta\end{bmatrix} d\theta d\bar{y} \tag{13}$$

where a_h is the attitude angle defined by the Eq. (14).

$$\alpha_h = \tan^{-1}\left(\frac{\bar{z} + 2\dot{\bar{x}}}{\bar{x} - 2\dot{\bar{z}}}\right) - \frac{\pi}{2}\operatorname{sign}\left(\frac{\bar{z} + 2\dot{\bar{x}}}{\bar{x} - 2\dot{\bar{z}}}\right) - \frac{\pi}{2}\operatorname{sign}(\bar{z} + 2\dot{\bar{x}}) \tag{14}$$

In order to find the analytical expression for the hydrodynamic forces, the solution of the integral G_h (Eq. (15)) is used to solve the Eq. (13) as shown below.

$$G_h = \int_{\alpha_h}^{\alpha_h+\pi} \frac{1}{1 - \bar{x}\cos\theta - \bar{z}\sin\theta} d\theta = \frac{2}{(1 - \bar{x}^2 - \bar{z}^2)^{1/2}}\left[\frac{\pi}{2} + \tan^{-1}\left(\frac{\bar{z}\cos\alpha_h - \bar{x}\sin\alpha_h}{(1 - \bar{x}^2 - \bar{z}^2)^{1/2}}\right)\right] \tag{15}$$

Therefore, the hydrodynamic force vector F$_h$ is given by:

$$F_h = -\mu\Omega\frac{RL_h^{\ 3}}{4C^2}\frac{\left[(\bar{z} + 2\dot{\bar{x}})^2 + (\bar{x} - 2\dot{\bar{z}})^2\right]^{1/2}}{1 - \bar{x}^2 - \bar{z}^2}\begin{bmatrix}3\bar{x}V_h - G_h\sin\alpha_h - 2S_h\cos\alpha_h \\ 3\bar{z}V_h + G_h\cos\alpha_h - 2S_h\sin\alpha_h\end{bmatrix} \tag{16}$$

where V_h and S_h are defined as:

$$V_h = \frac{2 + (\bar{z}\cos\alpha_h - \bar{x}\sin\alpha_h)G_h}{1 - \bar{x}^2 - \bar{z}^2} \tag{17}$$

$$S_h = \frac{\bar{x}\cos\alpha_h + \bar{z}\sin\alpha_h}{1 - (\bar{x}\cos\alpha_h + \bar{z}\sin\alpha_h)^{1/2}} \tag{18}$$

5 SIMULATED ANNEALING

The optimization method known as Simulated Annealing belongs to the class methods that attempt to simulate the processes used by nature to solve complex optimization problems. According to Faria and Saramago (2001), this technique is based on the analogy that is found when considering the growth of a single crystal of a molten metal, which corresponds to finding the local minimum of internal metal energy (objective function), this being a function of arrangement of atoms (variables project).

When the metal is cooled under appropriate conditions, it is possible to obtain the single crystal. In the process of annealing, first the metal is taken to high temperatures, causing vibration (shaken) of the atoms. If the material is cooled very quickly, the microstructure tends to a random and unstable form. However, if it is cooled properly and slowly, the microstructure tends to be arranged in a stable and orderly fashion. Analogously, in the optimization method based on metallurgy the design variables are disturbed randomly and the best value of the objective function is kept for each disturbance. After that, the temperature is reduced (annealing) and a new search is performed. The optimization process continues iteratively until convergence is reached. Figure 2 presents the analogy between the optimization process and simulated annealing. The method is able to determine global minima solutions searching the most stable position for the crystals of the material, which is analogous to the minimum value of the objective function.

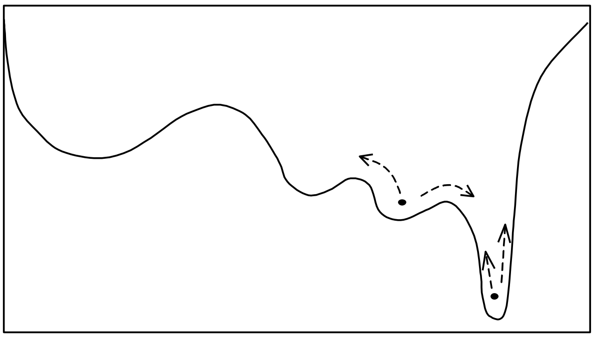

Figure 2. Analogy between the optimization process and simulated annealing (Saramago, 2003).

In this work, the algorithm developed by Carvalho and Saramago (2014) will be used. In this case, the traditional simulated annealing method is improved with some modifications aiming at reducing the associated computational costs. According to the authors, the proposed changes avoid unnecessary iterations that control the stagnation.

6 NUMERICAL RESULTS

The proposed analysis was applied to a horizontal rotating machine modeled by using 35 Timoshenko beam elements, as shown in Fig. 3. The finite element model is composed by a flexible steel shaft with 833 mm length and 19.05 mm diameter (E = 1.92 x 10^{11} Pa, ρ = 8000 kg/m^3, and υ = 0.29), three rigid discs D_1 (node #16; 0.658 kg), D_2 (node #20; 5.013 kg), and D_3 (node #25; 0.658 kg); and two cylindrical hydrodynamic bearings (B_1 and B_2, located at the nodes #9 and #35, respectively), each one with 19.05 mm diameter and 12.8 mm length.

A model updating procedure was used in order to obtain a representative FE model of the system. In this sense, the Simulated Annealing optimization technique was used to determine the unknown parameters of the model, namely the proportional damping added to the matrix D (Eq. (1); coefficients α and β; $D_p = \alpha\ M + \beta\ K$) and the additional stiffness associated with the coupling of the disc D_2 with the shaft. In this case, the diameter of the shaft at the disc location (i.e., elements #19 and #20; see Fig. 3) was considered as an additional unknown parameter, as proposed by Lalanne and Ferraris (1998). The entire frequency domain process (i.e. comparison between simulated and experimental frequency response functions, FRF) was performed 10 times, considering 20 individuals in the initial population of the optimizer. The objective function adopted is similar to the one presented in Eq. (17). However, in this case only the regions close to the peaks associated with the natural frequencies were taken into account.

The experimental FRFs were measured on the rotating system for the free-free condition by applying impact forces along the horizontal direction of the nodes #4, #11, #18, #27 and #34 separately. The response signals were measured by an accelerometer installed along the same direction of the impact forces at node #34, resulting in five FRFs. The measurements were performed by a signal analyzer, *Agilent*® (model 35670A), in a range from 0 to 300 Hz and steps of 0.5 Hz.

a) Rotating machine.

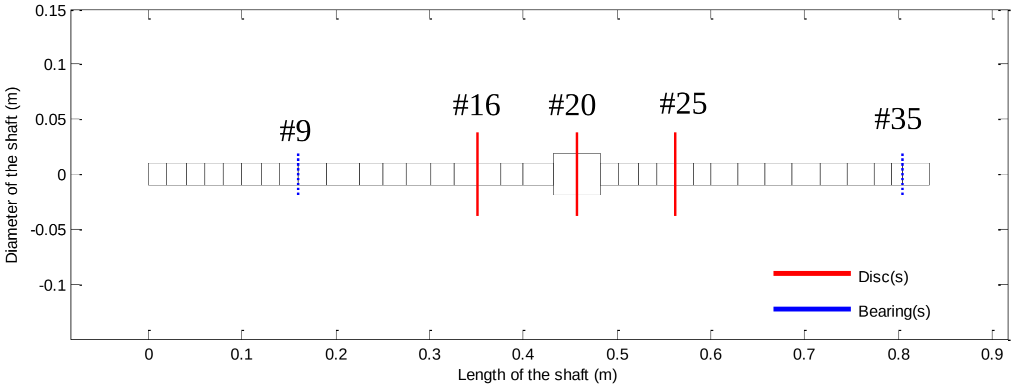

b) FE model.

Figure 3. Flexible rotor used on the numerical and experimental analysis.

Table 1 summarizes the parameters determined in the end of the minimization process associated with the smaller fitness value (i.e. value of the objective function) and the lower and upper limits imposed to the optimization process. Figure 4a and Fig. 4b compares two simulated and experimental FRFs (obtained from impacts on nodes #4 and #34, respectively) by considering the optimized parameters shown in Tab. 1. Note that the FRFs generated from the FE model are satisfactorily close to the ones obtained directly from the test rig.

Table 1. Parameters determined by the model updating procedure.

Parameters	Lower limit	Upper limit	Optimized values
α	$1 \, x \, 10^{-3}$	5	4.8008
β	$1 \, x \, 10^{-5}$	$1 \, x \, 10^{-2}$	$1.1306 \, x \, 10^{-5}$
Shaft diameter (m)	$9.525 \, x \, 10^{-3}$	$3.81 \, x \, 10^{-2}$	$1.876 \, x \, 10^{-2}$

Concerning now the assembled test rig (i.e., rotor under operating condition), displacement responses are collected in the vicinity of the bearings locations (measurement planes S_1 and S_2; nodes #10 and #33, respectively) along the horizontal and vertical directions (X and Z, respectively). Unbalance masses of 450 g.mm / 0^o were applied to the discs D_1 and D_3, respectively. The radial clearance of the bearings B_1 and B_2 were taken as C = 152.4 μm. The oil viscosity was considered equal to 0.0439 Pa.s (MINERAL OIL ISO 13 at 23^{o}C).

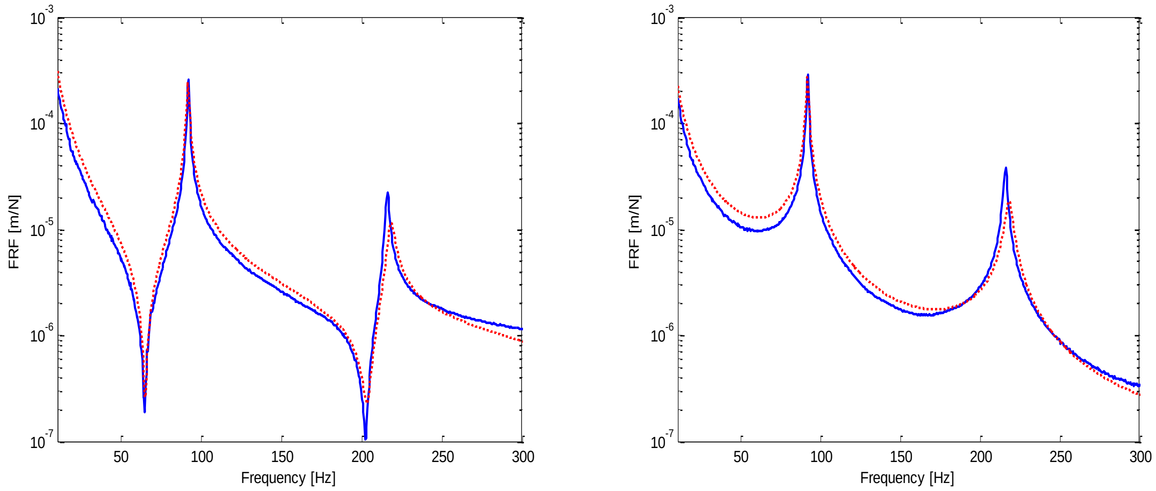

a) Impact on the node #4.
b) Impact on the node #34.

Figure 4. Simulated (- - -) and experimental (----) FRF.

Figure 5 compares the orbits obtained from the linear and nonlinear theories considering the unbalance, the properties of the bearings, and the rotor speed mentioned above. As expected, it can be observed that the rotor responses changes according with the used theory. The hypothesis of short sleeve bearing is based on the relationship $L_h/2R \leq 0.5$ (Meggiolaro, 1996). However, in this case $L_h/2R$ = 0.0128/0.01905 = 0.672 (dimensions in mm). It is worth mentioning that the displacement responses obtained from the nonlinear theory is devoted to short bearings, while the linear theory is derived considering the bearing as being long (Riul, 1992; see Eq. (2) and Eq. (10)). However, note that the amplitude of the responses determined along the horizontal and vertical directions seems to be similar.

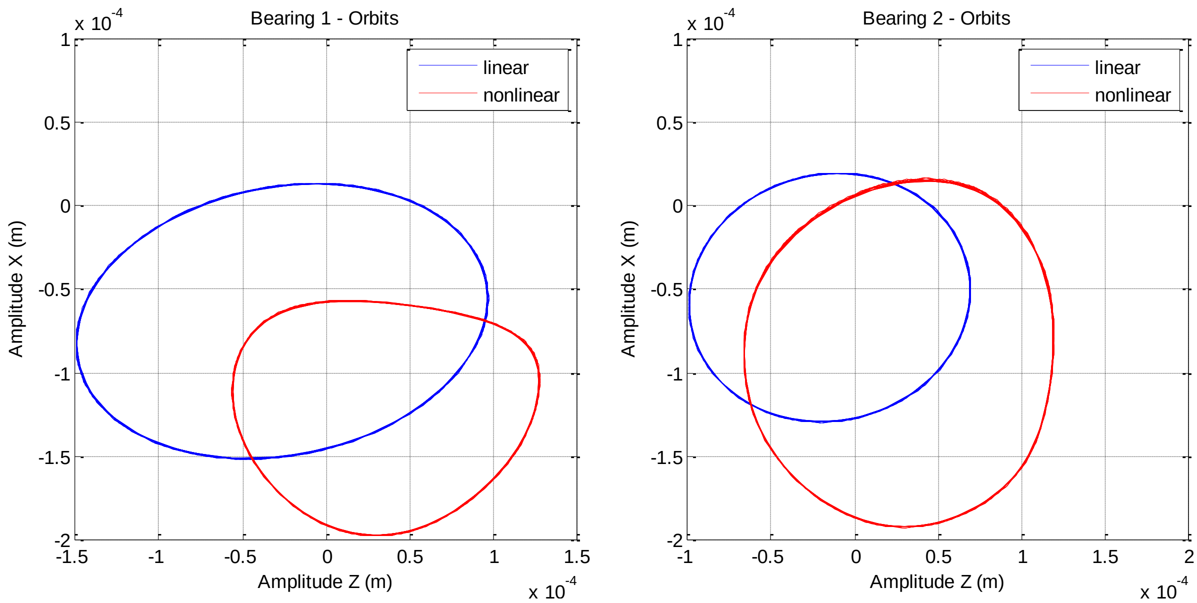

a) Measuring plane S_1.
b) Measuring plane S_2.

Figure 5. Orbits obtained from the linear and nonlinear theories.

Figure 6 illustrates the displacements obtained from the measuring planes S_1 and S_2 with the rotor in a linear run-down condition from 500 to 2240 rev/min in 10 sec. Both linear and nonlinear models for the bearings are considered. It can be observed that the two first critical speeds (backward and forward) of the rotating machine are, approximately, 1605 RPM and 1920 RPM considering the bearings modeled from the linear theory. Concerning the nonlinear theory, the associated critical speeds are, approximately, 1650 RPM and 1890 RPM.

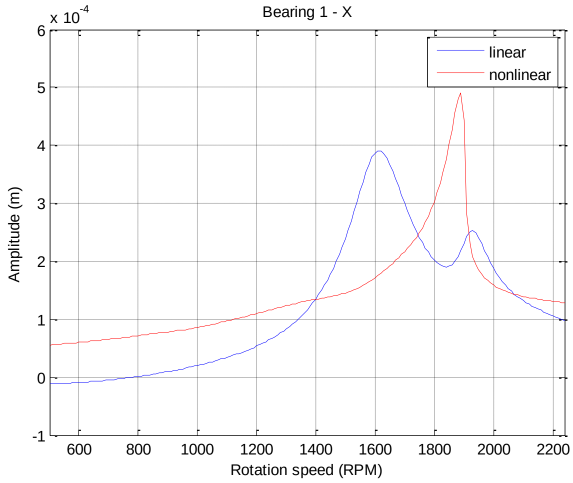

a) Measuring plane S_1 – X direction.

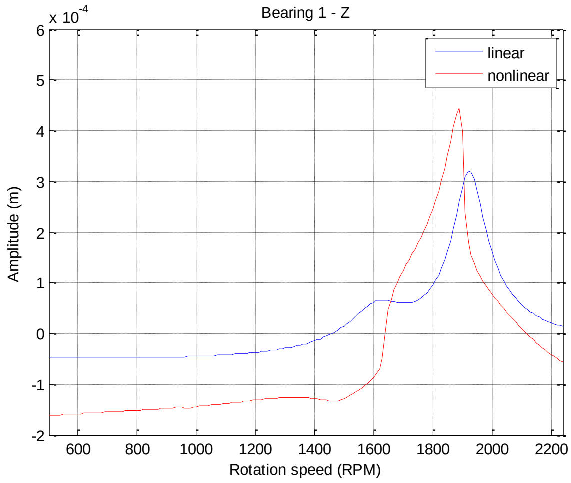

b) Measuring plane S_1 – Z direction.

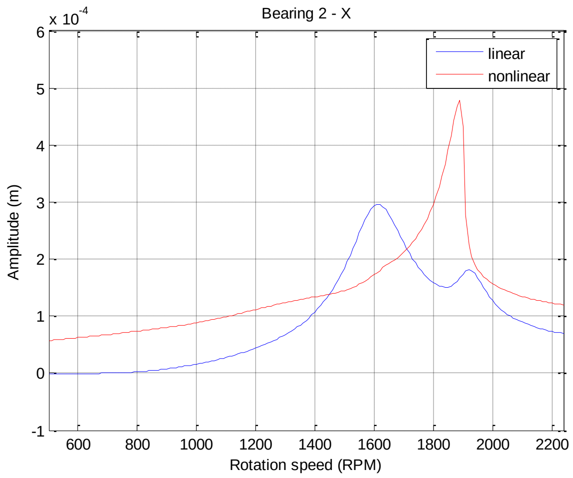

c) Measuring plane S_2 – X direction.

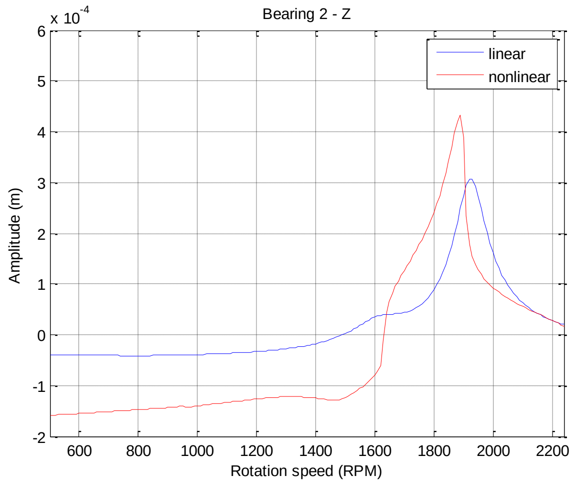

d) Measuring plane S_2 – Z direction.

Figure 6. Unbalance responses of the rotor operating in a linear run-up condition.

The critical speeds observed on the unbalance responses of the Fig. 6a and Fig. 6b (linear theory) are verified on associated Campbell's diagram presented in Fig. 7. Clearly, the Campbell's diagram was determined considering the same linear theory.

Figure 8 presents the Campbell's diagram determined by using the nonlinear bearing theory. Considering the rotor operating at a given rotation speed, horizontal forces of 1 N with different frequencies (from 0 to 50 Hz in steps of 1 Hz) were applied separately on node #20 of the FE model (see Fig. 3). In this case, the associated output responses were obtained along the horizontal direction of the same node. This procedure was performed for various rotation speeds (from 400 to 2500 RPM in steps of 100 RPM) in order to determine the diagram.

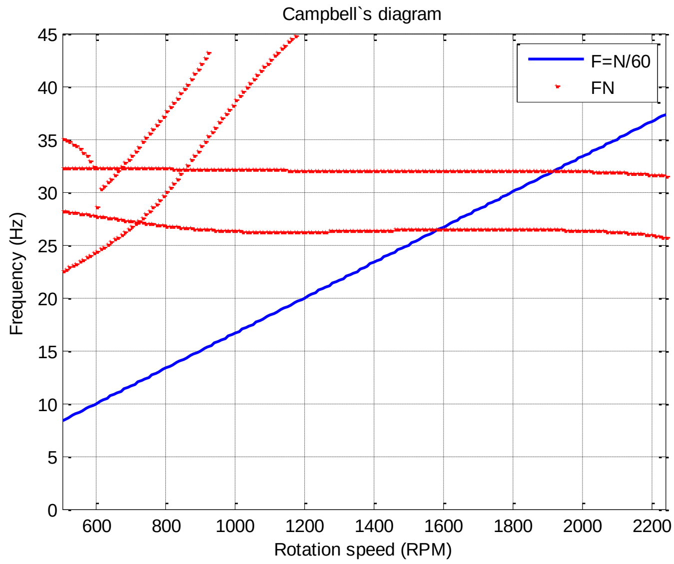

Figure 7. Campbell's diagram determined by using the linear bearing theory.

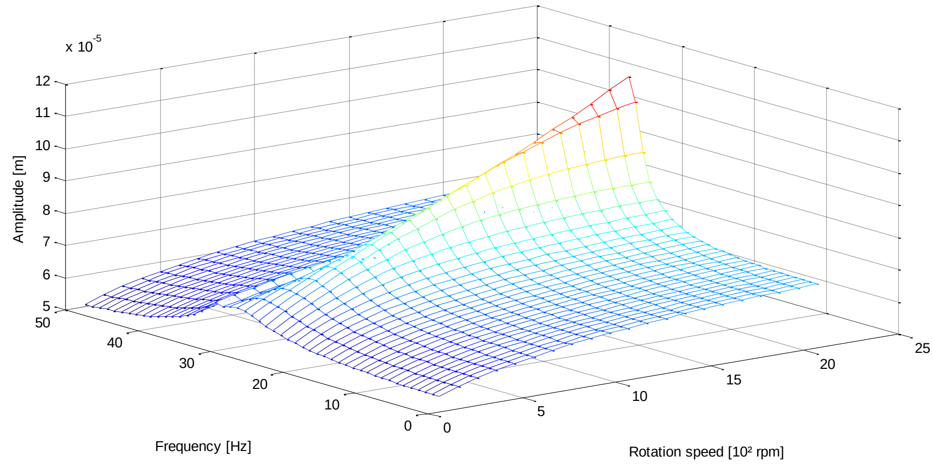

a) 3D view.

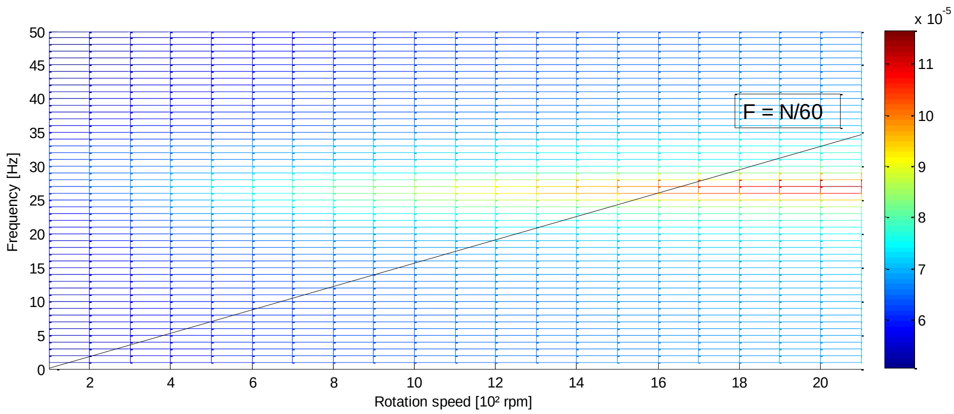

b) 2D superior view.

Figure 8. Campbell's diagram determined by using the nonlinear bearing theory.

7 CONCLUSION

In this paper, the linear and nonlinear approaches were used to model cylindrical hydrodynamic bearings. For the linear theory, the pressure field and, consequently, the supporting forces are determined from the solution of the Reynolds' equation for long bearings. The finite difference method is used to obtain the pressure field along the oil film. The stiffness and damping coefficients that represent the bearings are obtained by moving the shaft from its equilibrium location. The supporting forces are determined directly when the nonlinear model is used. It is worth mentioning that this theory is devoted only to short bearings. As expected, some differences could be observed on the vibration responses of the rotor associated with the linear and nonlinear models of the bearings. Both models lead to similar critical speeds, being the major discrepancies observed on the vibration amplitudes. Further studies will encompass an experimental verification of the determined results.

ACKNOWLEDGEMENTS

The authors are thankful to the Brazilian Research Agencies FAPEMIG and CNPq (INCT-EIE) and to CAPES for the financial support provided to this research effort.

REFERENCES

Capone, G., 1986 *Orbital Motions of Rigid Symmetric Rotor Supported on Journal Bearings*. La Meccanica Italiana, Vol. 199, pp. 37-46.

Carvalho, V. N., & Saramago, S. F. P., 2014. *Improved Simulared Anneling*. CNMAI.

Faria, E. D., & Saramago, S.F.P., 2001. *Constraint Optimization Problems Using Simulated Annealing*. Science & Engineering, Brazil, Vol. 10, n. 1, pp. 69-75.

Lalanne, M., & Ferraris,G., 1998. *Rotordynamics Prediction in Engineering.* John Wiley & Sons, INC.

Meggiolaro, M. A.,1996. *Modelagem de Mancais Hidrodinâmicos na Simulação de Sistemas Rotativos*. Pontifícia Universidade Católica do Rio de Janeiro.

Saramago, S.F.P., 2003. *Random Optimization methods: Genetic Algorithms and Simulated Annealing*, CNMAC.

Riul, J. A., Steffen Jr, V., & Ribeiro, C. R., 1992. *Estudo Teórico de Mancais Hidrodinâmicos Cilíndricos.* Revista Brasileira de Ciências Mecânicas, Vol. XIV, pp. 17-40.

Riul, J. A., 1988. Estudo Teórico e Experimental de Mancais Hidrodinâmicos Cilíndricos. Universidade Federal de Uberlândia.

Vance, J. M., Zeidan, F. Y., & Murphy, B., 2010. *Machinery Vibration and Rotordynamics*. John Wiley & Sons, INC.